



Power Electronic Systems  
Laboratory

© 2013 IEEE

IEEE Transactions on Power Electronics, Vol. 28, No. 8, pp. 4074-4082, August 2013

## Current Control of Three-Phase Rectifier Systems Using Three Independent Current Controllers

M. Hartmann,  
H. Ertl,  
J. W. Kolar

This material is published in order to provide access to research results of the Power Electronic Systems Laboratory / D-ITET / ETH Zurich. Internal or personal use of this material is permitted. However, permission to reprint/republish this material for advertising or promotional purposes or for creating new collective works for resale or redistribution must be obtained from the copyright holder. By choosing to view this document, you agree to all provisions of the copyright laws protecting it.



Eidgenössische Technische Hochschule Zürich  
Swiss Federal Institute of Technology Zurich

# Current Control of Three-Phase Rectifier Systems Using Three Independent Current Controllers

Michael Hartmann, *Member, IEEE*, Hans Ertl, *Member, IEEE*, and Johann W. Kolar, *Fellow, IEEE*

**Abstract**—Three-phase rectifier systems without connection of the neutral wire are characterized by the coupling of the phase input currents. Considering these couplings requires a transformation of the system equations into a static  $\alpha\beta$ -frame or into the rotating  $dq$ -reference frame where instead of the three coupled phase currents two independent current components are controlled. In this paper, it is shown that, despite of the existing cross-couplings, three independent phase current controllers can be used to control the system. Thereto, the cross coupling elements of the system transfer matrix have to fulfill some requirements which are derived using the Gershgorin theorem. The three-phase  $\Delta$ -switch rectifier circuit is used for analysis and a detailed model of the rectifier system is derived where the cross couplings are visible. The model is subsequently used to evaluate the cross couplings and three independent current controllers are designed. Simulation and experimental results verify the control approach using three independent current controller for three-phase rectifier systems.

**Index Terms**—Current control, power factor correction, three-phase ac/dc converter.

## I. INTRODUCTION

INTERCONNECTION of power electronics to the grid has in a wide range been performed using passive three-phase rectifier circuits in combination with inductors located either on the ac or on the dc-side. These rectifier circuits are simple, show a high efficiency and are very robust, but result in a total harmonic distortion (THD<sub>i</sub>) of the input currents of typically 30–50% and show a considerably small power factor. Due to upcoming standards containing rigorous input current harmonic limits such as the airborne standard DO160F [1], passive rectifier systems cannot be used anymore and either hybrid or active three-phase rectifier systems have to be applied instead [2]. Active three-phase PWM-rectifiers offer unity power factor, a THD<sub>i</sub> below 5% and a high power density. In many applications, energy feedback into the mains is not required or even not

allowed and unidirectional rectifier systems such as the Vienna Rectifier [3] or the  $\Delta$ -switch rectifier [4] may be used instead.

The high input current quality of a THD<sub>i</sub> below 5% is achieved by proper control of the rectifier circuit. A survey on current control methods of active three-phase PWM-rectifier systems can be found in [5]. Whereas the direct power control approach [6], [7] uses active and reactive power to directly generate the switching patterns, most control approaches are based on input currents of the rectifier. Due to possible disturbances and voltage spikes coming from the grid, the guidance of the input currents is essential and approaches using direct control of the input currents seems to be the better solution for rectifier systems.

Many control approaches avoid the time-variant behavior of the current control loop quantities by transferring the state variables of the system into the  $dq$ -space by application of the Park transformation [8], [9]. This means that some information on the mains frequency and the mains voltage phase angle are required and such a controller might therefore not operate as intended in case of a single phase loss.

A hysteresis controller as shown in [10] and [11] would be an effective way to control the rectifier system but its varying switching frequency increases the effort of EMI filtering. A controller implementation using the one cycle control method is presented in [12] and [13] which limits the control to always only two phases but there the controller structure has to be changed over every 60°.

In [14], a PWM control method for the  $\Delta$ -switch rectifier circuit has been proposed and in [4] a more detailed analysis of the switching sequences is given and a simultaneous phase-related current control of all three phase is proposed. There, three independent current controllers, one for each phase, are used to control the input currents. It is, however, prior not self-evident that this approach yields to a proper and stable current controller design as only two of the three boost inductors represent independent energy storage elements due to the missing neutral point connection of the rectifier system. In this paper, this control approach is analyzed in detail using the three-phase unidirectional  $\Delta$ -switch rectifier circuit and it is shown that this approach yields good results as long as some boundary conditions are fulfilled. It is, however, important to mention that the derived results are not only valid for the  $\Delta$ -switch rectifier circuit but for similar active PWM three-phase rectifier systems such as the Vienna Rectifier.

In Section II, a short description of the  $\Delta$ -switch rectifier circuit is given and in Section III, a phase-related model of the three-phase rectifier circuit is derived. The design of a single input single output (SISO) controller is discussed in Section IV, and in Section V, simulation results of the proposed controller

Manuscript received May 9, 2012; revised August 29, 2012; accepted November 18, 2012. Date of current version January 18, 2013. Recommended for publication by Associate Editor Dr. M. Liserre.

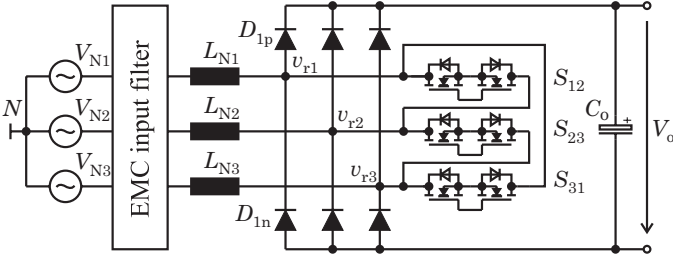
M. Hartmann was with the Power Electronic Systems Laboratory, Eidgenössische Technische Hochschule Zürich, 8092 Zürich, Switzerland. He is now with Schneider Electric, Drive Technology and Systems, A-1210 Vienna, Austria (e-mail: michael.hartmann@ieee.org).

H. Ertl is with the Power Electronics Section, Vienna University of Technology, A-1040 Vienna, Austria (e-mail: j.ertl@tuwien.ac.at).

J. W. Kolar is Head of the Power Electronic Systems Laboratory, Eidgenössische Technische Hochschule Zürich, 8092 Zurich, Switzerland (e-mail: kolar@lem.ee.ethz.ch).

Color versions of one or more of the figures in this paper are available online at <http://ieeexplore.ieee.org>.

Digital Object Identifier 10.1109/TPEL.2012.2231946

Fig. 1. Schematic of the two-level three-phase  $\Delta$ -switch rectifier.

are presented. The design concept is verified in Section IV by measurements taken from a 10-kW hardware prototype.

## II. THREE-PHASE $\Delta$ -SWITCH RECTIFIER SYSTEM

The basic schematic of the three-phase  $\Delta$ -switch rectifier system is depicted in Fig. 1. The system consists of a three-phase diode bridge and three bidirectional (current) bipolar (voltage) switches  $S_{ij}$  ( $i, j \in \{1, 2, 3\}$ ) which are connected between the phases ( $\Delta$ -connection). The three boost inductors  $L_{Ni}$  are connected to the input of the rectifier bridge. Together with the boost inductors the three switches  $S_{ij}$  are used to generate sinusoidal input currents which are proportional to the mains voltage. Due to the rectifier diodes, a short-circuit of the dc-link voltage is not possible. In contrast to a conventional rectifier bridge the diodes commute with switching frequency and have to be chosen according to this requirement. In Fig. 1, bidirectional switch implementation using back-to-back connected MOSFETs is shown. It has to be stated here that MOSFETs with a blocking voltage of 650 V can only be applied if the rectifier system is designed for a mains voltage of 200 V. Due to the two-level characteristic of the  $\Delta$ -switch topology 1200-V IGBTs and 1200-V diodes have to be used for a mains voltage of 400 V.

The  $\Delta$ -switch rectifier circuit can only generate discrete voltage space vectors which are used to approximate the converter's voltage reference vector  $\underline{v}_r$  in the time average over the pulse period. This yields, in connection with the mains voltage space vector  $\underline{v}_N$  to an appropriate input current  $\underline{i}_N$  (more details can be found in [4]). The total available voltage space vectors are depicted in Fig. 2. Each vector is marked with  $(s_{12}, s_{23}, s_{32})(\text{sign}(i_{N1}), \text{sign}(i_{N2}), \text{sign}(i_{N3}))$  where 1 means that the corresponding switch  $S_{ij}$  is turned ON and 0 that it is turned OFF. The current direction is marked with  $+/-$  for currents flowing into/out of the rectifier system and x designates that the vector is independent of the current direction of the corresponding phase. All voltage space vectors with two or three switches in the on-state short all three input phases on the rectifier side and are therefore redundant. This redundancy cannot be used advantageously and only two switches can hence be used to control the input currents. The remaining switch has to be permanently OFF during this  $60^\circ$ -sector. The required clamping actions considering all  $60^\circ$ -sectors are summarized in Table I for all MOSFETs, where, i.e., 0 indicates that the corresponding MOSFET is permanently off in this sector.

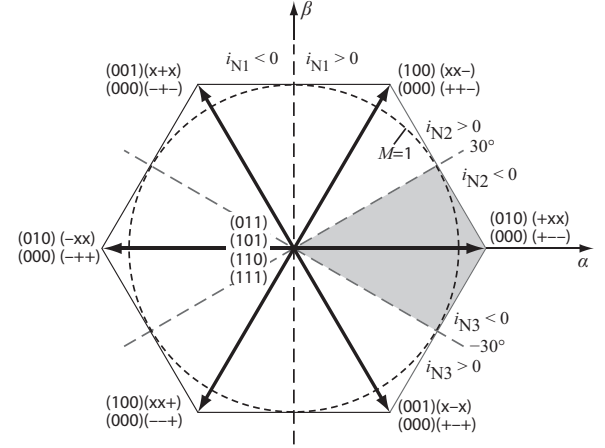


Fig. 2. Total available voltage space vectors of the  $\Delta$ -switch rectifier system. Depending on the input phase current directions only four voltage space vectors can be generated. Each vector is marked with  $(s_{12}, s_{23}, s_{32})(\text{sign}(i_{N1}), \text{sign}(i_{N2}), \text{sign}(i_{N3}))$ .

TABLE I  
REQUIRED CLAMPING ACTIONS; 0 INDICATES THAT THE CORRESPONDING MOSFET IS OFF FOR THE WHOLE INTERVAL; 1 INDICATES A CONTINUOUS TURN ON IN THE CONSIDERED INTERVAL AND PWM<sub>ij</sub> THAT THE MOSFET IS MODULATED BY THE CURRENT CONTROLLER

	$s_{12}$	$s_{21}$	$s_{23}$	$s_{32}$	$s_{13}$	$s_{31}$
$330^\circ \dots 30^\circ$	$pwm_{12}$	1	0	0	$pwm_{13}$	1
$30^\circ \dots 90^\circ$	0	0	$pwm_{23}$	1	$pwm_{13}$	1
$90^\circ \dots 150^\circ$	1	$pwm_{21}$	$pwm_{23}$	1	0	0
$150^\circ \dots 210^\circ$	1	$pwm_{21}$	0	0	1	$pwm_{31}$
$210^\circ \dots 270^\circ$	0	0	1	$pwm_{32}$	1	$pwm_{31}$
$270^\circ \dots 330^\circ$	$pwm_{12}$	1	1	$pwm_{32}$	0	0

The basic structure of the controller used in this study is shown in Fig. 3 and has been proposed in [4]. All three input currents  $i_{Ni}$  are sensed by appropriate current sensors and compared with the corresponding reference currents  $i_{Ni}^*$ . The reference currents are generated by multiplying the mains voltages  $v_{Ni}$  by a reference conductance  $G_e^*$  which is defined by the superimposed output voltage controller  $K_V(s)$ . The output voltage controller is typically implemented as a PI-type controller in order to avoid a steady state control error. Due to the multiplication with the conductance  $G_e^*$ , ohmic input current behavior is achieved. Together with a mains voltage feedforward signal [15], the current controller  $K_I(s)$ , which shall be implemented as a P-type controller, generates the phase-related modulations signals  $m_i$  which finally yield to the required converter phase voltages  $v_{ri}$ . The bidirectional switches are connected between two phases and therefore the equivalent line-to-line modulations signals are required for PWM generation which correspond to the line-to-line voltages  $v_{ij}$  (see also [4]).

The star- $\Delta$  transformation is followed by two pulse-width modulators which generate the PWM signals for the MOSFETs of the bidirectional switches. In general, dependent on the current direction of the bidirectional switch, only one MOSFET has to be gated. If the second MOSFET is permanently OFF during this time, the current is carried by its body diode and the

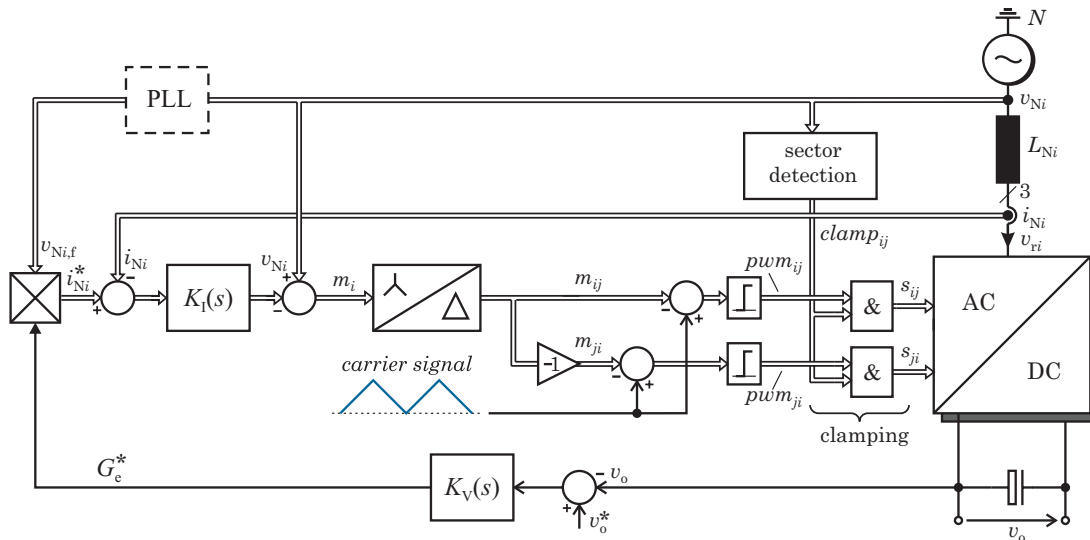


Fig. 3. Structure of the cascaded control proposed in [4] including the phase-oriented PWM current control. Signal paths being equal for all three phases are shown by double lines.

relative large forward voltage drop yields to higher conduction losses which could be reduced if the second MOSFET is turned ON as well. The current direction of the switch only changes every  $120^\circ$  and this MOSFET can therefore be permanently on during this time interval. Two independent PWM signals are hence required for the bidirectional switches.

The presented controller structure achieves ohmic input behavior by multiplying the measured phase voltages with a conductance  $G_e^*$ . This simple approach would, however, result in input current distortions in case of a distorted grid voltage which can typically not be tolerated. A PLL as shown in [16] and indicated in Fig. 3 or tuned band passes can therefore be used to generate reference voltages containing only the fundamental component of the grid voltage. This is, however, not easily possible in case of a variable mains frequency as it may occur in aerospace applications where the mains frequency can vary between 360 and 800 Hz.

### III. CONVERTER MODEL

The proposed controller structure uses decoupled models for the ac-side of the rectifier system (current control) and dc-side of the rectifier system (output voltage control). The decoupling of the voltage and current control loop is justifiable by the different dynamic behaviors of both sides. The time behavior of the current control loop is related to the switching frequency  $f_s$  where the output voltage control is related to the mains frequency  $f_N$  which is considerably lower than  $f_s$ . The typically relative large output capacitor  $C_o$  is the decoupling element of the two control loops and a cascade control structure can therefore be used. In this paper, only the design of the current controller is discussed, whereas the design of the superimposed voltage control loop can be found in [17].

In order to be able to design a proper current controller an adequate model of the rectifier system is required. The digital controller will be implemented using a DSP and sampling effects and delay times caused by the calculation time of this digital

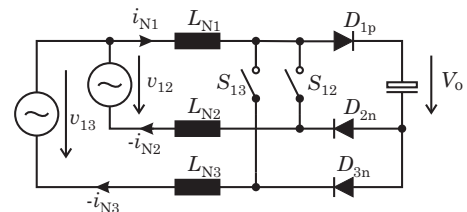


Fig. 4. Equivalent dual-boost circuit for  $\varphi_N \in [-30^\circ, +30^\circ]$ .

implementation have to be considered for the stability analysis of the controller loop. Due to sampling of the analog signals the phase margin of the system is reduced considerably and a system model neglecting these effects will not yield to an optimal control of the rectifier system.

The three switches of the  $\Delta$ -switch rectifier system are connected between the phases which means that all three currents are directly affected by the switching action of one bidirectional switch. Due to the high redundancy of voltage space vectors one switch is always continuously clamped to the off-state in a  $60^\circ$ -sector. An equivalent circuit consisting of two boost circuits (dual-boost circuit), as already shown in [12], can be drawn for each sector. Fig. 4 shows the resulting dual boost circuit for  $\varphi_N \in [-30^\circ, +30^\circ]$ . The input voltages  $v_{12}$  and  $v_{13}$  show positive values and the input current  $i_{N1}$  shows positive direction whereas the input currents  $i_{N2}$  and  $i_{N3}$  show negative direction. Switches  $S_{12}$  and  $S_{13}$  are pulse-width modulated and according to Table I the switches  $S_{23}$  and  $S_{32}$  are clamped to the off-state. It is obvious that the boost inductor  $L_{N1}$  and the rectifier diode  $D_{1p}$  are shared by the two virtual boost circuits.

An analysis of all sectors shows that for each sector a corresponding equivalent dual-boost circuit similar to the circuit given in Fig. 4 can be derived. The corresponding equivalent dual-boost circuits and the resulting parameters of the elements for each sector are listed in Table II.

TABLE II  
EQUIVALENT DUAL-BOOST CIRCUITS OF THE  $\Delta$ -SWITCH RECTIFIER AND CORRESPONDING CIRCUIT ELEMENTS FOR EACH  $60^\circ$ -SECTOR

$\varphi_N$	Circuit	$v_\alpha$	$v_\beta$	$L_A$	$L_B$	$L_C$	$S_\alpha$	$S_\beta$	$D_A$	$D_B$	$D_C$
$-30^\circ \dots 30^\circ$	C <sub>2</sub>	$v_{12}$	$v_{13}$	$L_{N2}$	$L_{N3}$	$L_{N1}$	$S_{12}$	$S_{13}$	$D_{2n}$	$D_{3n}$	$D_{1p}$
$30^\circ \dots 90^\circ$	C <sub>1</sub>	$v_{13}$	$v_{23}$	$L_{N1}$	$L_{N2}$	$L_{N3}$	$S_{13}$	$S_{23}$	$D_{1p}$	$D_{2p}$	$D_{3n}$
$90^\circ \dots 150^\circ$	C <sub>2</sub>	$v_{21}$	$v_{23}$	$L_{N1}$	$L_{N3}$	$L_{N2}$	$S_{21}$	$S_{23}$	$D_{1n}$	$D_{3n}$	$D_{2p}$
$150^\circ \dots 210^\circ$	C <sub>1</sub>	$v_{21}$	$v_{31}$	$L_{N2}$	$L_{N3}$	$L_{N1}$	$S_{21}$	$S_{31}$	$D_{2p}$	$D_{3p}$	$D_{1n}$
$210^\circ \dots 270^\circ$	C <sub>2</sub>	$v_{32}$	$v_{31}$	$L_{N2}$	$L_{N1}$	$L_{N3}$	$S_{32}$	$S_{31}$	$D_{2n}$	$D_{1n}$	$D_{3p}$
$270^\circ \dots 330^\circ$	C <sub>1</sub>	$v_{12}$	$v_{32}$	$L_{N1}$	$L_{N3}$	$L_{N2}$	$S_{12}$	$S_{32}$	$D_{1p}$	$D_{3p}$	$D_{2n}$

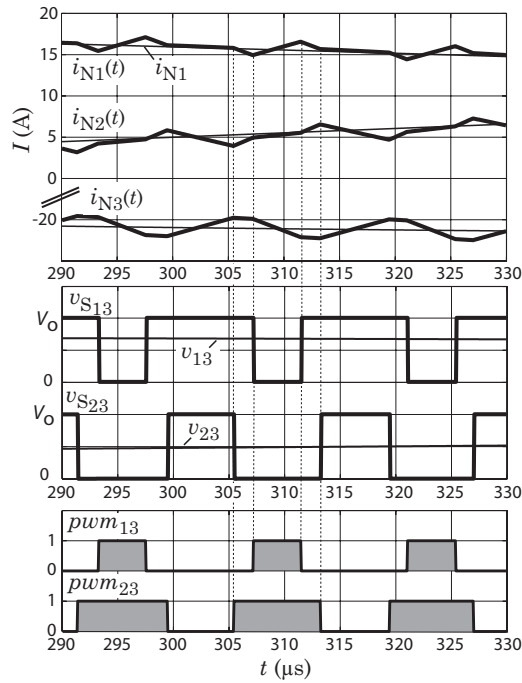


Fig. 5. Simulated voltage and current waveforms for  $\varphi_N = 45^\circ$  system parameters:  $V_N = 115$  V,  $V_o = 400$  V,  $f_N = 400$  Hz,  $L_N = 330 \mu\text{H}$  and  $P_o = 5$  kW).

In the following, a model for sector  $\varphi_N \in [30^\circ, 90^\circ]$  is derived. The approach can be applied in a similar manner to the other sectors.

Average mode current control will be used to control the rectifier system which means that all signals are averaged over one pulse period. In order to apply the average mode current control concept, the bandwidth of the controller must be chosen significantly lower than the switching frequency of the converter. Fig. 5 shows the simulated voltage and current waveforms around  $\varphi_N = 45^\circ$  ( $V_N = 115$  V,  $V_o = 400$  V,  $f_N = 400$  Hz,  $L_N = 330 \mu\text{H}$ , and  $P_o = 5$  kW), where  $v_{S_{13}}$  and  $v_{S_{23}}$  are the corresponding voltage waveforms of the bidirectional switches

and  $v_{13}$  and  $v_{23}$  are the line-to-line mains voltages. The averaged input current  $i_{N1, \text{avg}}$  for instance can be calculated using

$$i_{N1, \text{avg}} = \frac{1}{T_s} \int_0^{T_s} i_{N1}(t) dt \quad (1)$$

where  $T_s = 1/f_s$  is one pulse period. In the following, only  $i_{N1}$  is written instead of  $i_{N1, \text{avg}}$  for a better readability but means the averaged value over one pulse period. Averaging over one pulse period and application of Kirchoff's law on the circuit C1 given in Table II results in

$$\begin{aligned} v_{13} - L_{N1} \frac{di_{N1}}{dt} + L_{N3} \frac{di_{N3}}{dt} &= (1 - \delta_{13}) V_o \\ v_{23} - L_{N2} \frac{di_{N2}}{dt} + L_{N3} \frac{di_{N3}}{dt} &= (1 - \delta_{23}) V_o \end{aligned} \quad (2)$$

where  $(1 - \delta_{13}) V_o$  is the averaged voltage across switch  $S_{13}$ . The forward voltage drops of switches and diodes are neglected in (2). Due to the missing neutral wire connection in addition

$$i_{N1} + i_{N2} + i_{N3} = 0 \quad (3)$$

has to be satisfied. The output voltage controller ensures a constant output voltage  $V_o$  which is in most cases fulfilled (approximately even during load transients). In a first approach,  $V_o$  is assumed to be constant so that the nonlinear equation (2) gets linear. The Laplace transform can therefore be applied and if equal boost inductors  $L_{N1} = L_{N2} = L_{N3} = L_N$  are assumed (2) and (3) yield to

$$\begin{aligned} v_{13} - i_{N1} s L_N + i_{N3} s L_N &= (1 - \delta_{13}) V_o \\ v_{23} - i_{N2} s L_N + i_{N3} s L_N &= (1 - \delta_{23}) V_o \\ i_{N1} + i_{N2} + i_{N3} &= 0. \end{aligned} \quad (4)$$

This simplification yields to a simple model for current control where the impacts of output voltage variations or saturation effects of the boost inductors are not considered. Solving (4)

results in

$$\begin{aligned} \begin{pmatrix} i_{N1} \\ i_{N2} \\ i_{N3} \end{pmatrix} &= \frac{V_o}{sL_N} \frac{1}{3} \begin{pmatrix} 2 & -1 \\ -1 & 2 \\ -1 & -1 \end{pmatrix} \begin{pmatrix} \delta_{13} \\ \delta_{23} \end{pmatrix} + \\ &+ \frac{1}{sL_N} \frac{1}{3} \begin{pmatrix} 2 & -1 \\ -1 & 2 \\ -1 & -1 \end{pmatrix} \begin{pmatrix} v_{13} \\ v_{23} \end{pmatrix} + \\ &+ \frac{V_o}{sL_N} \frac{1}{3} \begin{pmatrix} -1 \\ -1 \\ 2 \end{pmatrix}. \end{aligned} \quad (5)$$

According to (5), the input currents are dependent on the duty cycles  $\delta_{ij}$ , the line-to-line mains voltages  $v_{ij}$  and the output voltage  $V_o$ . Using the modulation function  $m_{ij}$ , the duty cycle is defined by

$$\delta_{ij} = 1 - m_{ij}. \quad (6)$$

The  $\Delta$ -related modulation functions are given by

$$m_{ij} = m_i - m_j \quad (7)$$

where the corresponding duty cycles of the virtual single-phase systems are

$$\delta_i = 1 - m_i. \quad (8)$$

In the final controller implementation, an input voltage feedforward part is used in conjunction with a P-type controller. The mains phase voltage  $v_i$ , related to the output voltage  $V_o$ , is there added to the output of the current controller  $m_i$

$$m_{i,ff} = \left( m_i + \frac{v_i}{V_o} \right). \quad (9)$$

After a short calculation the  $\Delta$ -related duty-cycles  $\delta_{ij}$  result in

$$\delta_{ij,ff} = 1 + \delta_i - \delta_j - \frac{v_{ij}}{V_o}. \quad (10)$$

By use of (10), the input currents can be described as a function of the phase related duty-cycles

$$\begin{aligned} \mathbf{i}_N &= \begin{pmatrix} i_{N1} \\ i_{N2} \\ i_{N3} \end{pmatrix} = \frac{V_o}{sL_N} \frac{1}{3} \begin{pmatrix} 2 & -1 & -1 \\ -1 & 2 & -1 \\ -1 & -1 & 2 \end{pmatrix} \begin{pmatrix} \delta_1 \\ \delta_2 \\ \delta_3 \end{pmatrix} \\ &= \mathbf{G}(s) \boldsymbol{\delta} \end{aligned} \quad (11)$$

where  $\mathbf{i}_N$  and  $\boldsymbol{\delta}$  are vectors and the  $3 \times 3$  matrix  $\mathbf{G}(s)$  is the multiple input/multiple output (MIMO) small signal average mode transfer function describing the  $\Delta$ -switch rectifier system.

It is obvious that not only the elements  $G_{ii}(s)$ , but also elements outside of the main diagonal  $G_{ij}(s)|_{i \neq j}$  are not zero. This means that for instance a change in the duty-cycle  $\delta_1$  does not only take effect just on the phase current  $i_{N1}$  but also on the phase currents  $i_{N2}$  and  $i_{N3}$ .

The reason for this strong coupling can be explained by use of (3). Due to the missing neutral connection of the rectifier system the sum of all three input currents is forced to zero. A change of the duty-cycle  $\delta_1$  therefore results in a change of input current  $i_{N1}$  which, however, also affects the currents  $i_{N2}$  and  $i_{N3}$ . Due

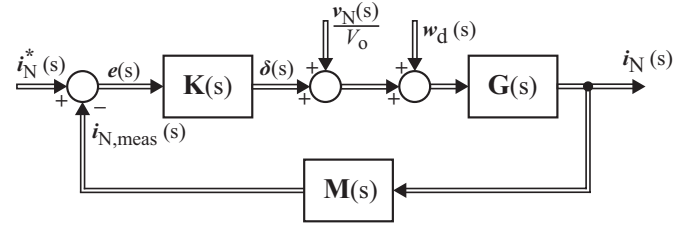


Fig. 6. Multiple-input multiple-output controller loop of the rectifier system consisting of the controller  $\mathbf{K}(s)$ , model of the rectifier system  $\mathbf{G}(s)$  and current measurement  $\mathbf{M}(s)$ . The vector  $\mathbf{w}_d(s)$  models a disturbance in the duty cycle.

to this circumstance the cross couplings are physical in nature and cannot be neglected *a priori*.

The elements in the main diagonal of  $\mathbf{G}(s)$  are equal and the elements outside of the principle diagonal are equal which results in a symmetrical system behavior. The step responses on  $\delta_1$  and the step responses on  $\delta_2$  are equal with respect to the corresponding phase current  $i_{Ni}$ .

The matrix  $\mathbf{G}(s)$  given in (11) was only derived for the sector  $\varphi_N \in [30^\circ, 90^\circ]$  and is only valid in this sector. However, due to the symmetry of the system all sectors result in the same transfer matrix (11) as can easily be verified by repetition of the calculation for other sectors.

#### IV. CONTROLLER DESIGN

Because of the nonzero nondiagonal elements of  $\mathbf{G}(s)$  in general a multivariable controller  $\mathbf{K}(s)$  ( $3 \times 3$  matrix) has to be designed. Nine controller elements  $K_{ij}(s)$  would have to be determined in order to implement a proper controller. The multivariable controller structure is depicted in Fig. 6, where  $\mathbf{G}(s)$  is the derived model of the rectifier system,  $\mathbf{K}(s)$  is the multivariable controller, and  $\mathbf{M}(s)$  is the transfer function of the current measurement. It is assumed that the measurement system shows no cross-couplings, hence  $\mathbf{M}(s)$  is a diagonal matrix. The vector  $\mathbf{w}_d(s)$  models a possible disturbance in the duty cycle generation (e.g., turn-off delays of the MOSFETs or deviations in the feed-forward voltage).

A return difference matrix

$$\mathbf{F}(s) = [\mathbf{I} + \mathbf{G}(s)\mathbf{K}(s)\mathbf{M}(s)] \quad (12)$$

of the multivariable control system can be defined which is used for controller design and for stability analysis.

A simple approach for controller design is to ignore the cross couplings of  $\mathbf{G}(s)$  in a first step. The multivariable control problem then simplifies to three independent single-input single-output (SISO) control systems according to the elements  $G_{ii}(s)$  and the influence of the remaining cross couplings have to be analyzed carefully after the controller elements have been designed. Fig. 7 illustrates the basic idea of this control method [18], [19]. The precondition for this control approach are loose cross couplings of  $\mathbf{G}(s)$  and the amount of cross coupling can be estimated by the calculation of the corresponding Gershgorin bands [18].

A design method using this basic idea has been developed by Rosenbrock [19] and is known as direct Nyquist array (DNA)

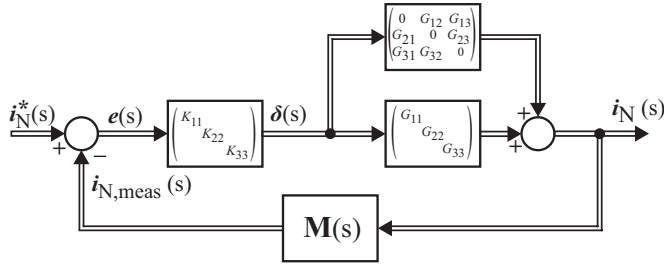


Fig. 7. Control loop illustrating the basic idea of the DNA control design method. The three controller elements  $K_{ii}(s)$  are designed according to the main diagonal elements  $G_{ii}(s)$ . The operating controller, however, has to deal with the full system  $\mathbf{G}(s)$ .

method. This method is used in the following for controller design and a summary of the method is given in the Appendix.

The measurement system in the easiest way can be modeled by a gain  $k_M$  typically representing the number of bits per ampere. The matrix  $\mathbf{M}(s)$  results in

$$\mathbf{M}(s) = \begin{pmatrix} k_M & 0 & 0 \\ 0 & k_M & 0 \\ 0 & 0 & k_M \end{pmatrix} \quad (13)$$

and together with the P-type controller matrix

$$\mathbf{K}(s) = \begin{pmatrix} k_p & 0 & 0 \\ 0 & k_p & 0 \\ 0 & 0 & k_p \end{pmatrix} \quad (14)$$

the return difference matrix (15), shown at the bottom of the page, can be calculated.

It is now assumed, that the P-type controller gain  $k_p$  is designed in such a way that the single-phase control loop is stable (details are discussed later). In a next step, the stability of the MIMO control system has to be checked by examining the return difference matrix  $\mathbf{F}(s)$ .

The elements of the return difference matrix given in (15) result in

$$\begin{aligned} |F_{ii}(j\omega)| &> \sum_{j=i, j \neq i}^m |F_{ij}(j\omega)| \\ \left| \frac{3j\omega L_N + 2k_p k_M V_o k_{pwm}}{3j\omega L_N} \right| &> \left| \frac{2k_p k_M V_o k_{pwm}}{3j\omega L_N} \right| \end{aligned} \quad (16)$$

for the  $\Delta$ -switch rectifier under investigation. Due to the term  $3j\omega L_N$  the matrix  $\mathbf{F}(s)$  is diagonally dominant and the MIMO control loop is stable. This means that three independent controllers can be designed using the diagonal elements  $G_{ii}(j\omega)$  and that the whole rectifier system is stable if the equivalent

single-phase control loops are stable. The DNA method, however, only assures stability and gives not information on the performance of the coupled control loops.

The derived result is not limited to the  $\Delta$ -switch topology and is a general result as more or less all three-phase converter circuits, e.g., such as the six-switch two-level rectifier circuit, the three-level neutral point clamped converter (NPC) or the Vienna Rectifier topology, show a similar structure as given in (11).

The DNA design method is not limited to a P-type controller structure and can in general be extended to PI-type or P-Resonant controllers. The requirement of diagonally row or column dominance of  $\mathbf{F}(s)$  [cf., (25) and (26)] may for these types of controllers only be fulfilled by a sufficiently small controller gain which may not be achieved easily. The stability criterion used by the direct Nyquist array method shown in Section A is, however, only sufficient and not required which means that the control loop may be stable although it does not fulfill the presented requirements. Alternative design methods optimized for PI-type controllers have thus been developed [18].

If diagonally row or column dominance of  $\mathbf{F}(s)$  cannot be achieved by a simple P-type controller a decoupling of the converter behavior can be done. A decoupling block

$$\mathbf{L}(s) = \mathbf{G}(s)^{-1} \text{diag}(G_i(s)) \quad (17)$$

is thereto located in front of the converter matrix  $\mathbf{G}(s)$  for full decoupling which transfers the coupled state variables into decoupled ones. Fully decoupling is only possible if the transfer functions  $G_i(s)$  show considerably high excess of poles, i.e., the number of poles of  $G_i(s)$  is considerably higher than the number of zeros of  $G_i(s)$ . This, however, would reduce the dynamic of the resulting plant and decoupling is therefore only used to achieve diagonal row or column dominance. Decoupling of the converter behavior is, however, not used for the case at hand.

As a next step, the controller elements  $K_{11}(s)$ ,  $K_{22}(s)$ , and  $K_{33}(s)$  have to be determined according to the diagonal elements  $G_{11}(s)$ ,  $G_{22}(s)$ , and  $G_{33}(s)$ . The three elements  $G_{ii}(s)$  are advantageously equal and the design of the three independent controllers can be reduced to the design of one controller. The control system will be implemented using a DSP and sampling effects and scaling constants have to be considered. The resulting (single-phase) control loop for the elements  $G_{11}(s)$  and  $K_{11}(s)$  is shown in Fig. 8 where the controller is given in its digital form  $K_{11}(z)$ . The digital redesign method of an analogue controller (cf., [20]), e.g., using the bilinear (Tustin) transformation for discretization can be used. A symmetrical PWM is applied and the phase currents are sampled at each

$$\mathbf{F}(s) = \mathbf{I} + \mathbf{G}(s)\mathbf{K}(s)\mathbf{M}(s) = \begin{pmatrix} \frac{3sL_N + 2k_p k_M V_o k_{pwm}}{3sL_N} & -\frac{k_p k_M V_o k_{pwm}}{3sL_N} & -\frac{k_p k_M V_o k_{pwm}}{3sL_N} \\ -\frac{k_p k_M V_o k_{pwm}}{3sL_N} & \frac{3sL_N + 2k_p k_M V_o k_{pwm}}{3sL_N} & -\frac{k_p k_M V_o k_{pwm}}{3sL_N} \\ -\frac{k_p k_M V_o k_{pwm}}{3sL_N} & -\frac{k_p k_M V_o k_{pwm}}{3sL_N} & \frac{3sL_N + 2k_p k_M V_o k_{pwm}}{3sL_N} \end{pmatrix} \quad (15)$$

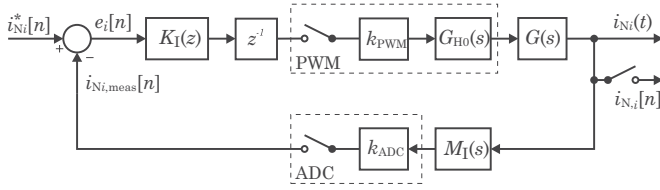


Fig. 8. Single-input single-output control loop of input current  $i_{N1}$  if the occurring cross couplings are neglected.

TABLE III  
SYSTEM PARAMETER FOR DESIGN OF THE CONTROLLER

Mains voltage:	$V_{LL} = 200$ V
Switching frequency:	$f_s = 72$ kHz
DC-link voltage:	$V_o = 400$ V
Boost inductor:	$L_N = 330$ $\mu$ H
Scaling measurement:	$k_m = 821$ Digits/A
Meas. time constant:	$T_M = 5$ $\mu$ s.
Scaling PWM:	$k_{pwm} = 11104$ Digits/Period $T_s$

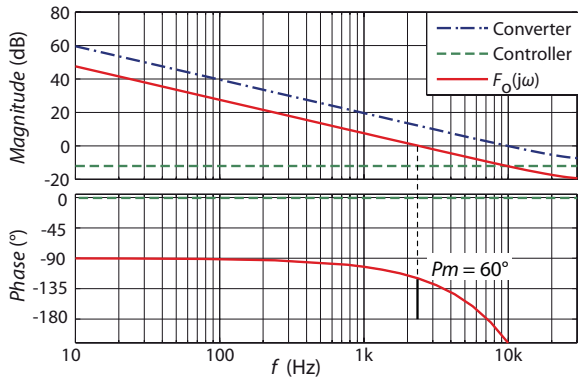


Fig. 9. Calculated Bode plot of the (digitalized) equivalent single-phase system. A P-type controller with a gain of  $k_p = 0.25$  leads to a phase margin of  $60^\circ$ .

peak value of the triangular-shaped carrier signal. The sampled current value is then equivalent to the current average value (see also [21]).

The delay of the symmetrical PWM is, according to [22], modeled by a sample and hold element  $G_{H0}(s)$  and the calculation delay of the digital controller implementation is considered by the block  $z^{-1}$ . The current sensor and analog measurement circuits contain a first-order low-pass filter (bandwidth limitation) and the more comprehensive model

$$M_{ii}(s) = \frac{k_m}{1 + sT_M} \quad (18)$$

where  $k_m$  is the number of digits per ampere and  $T_M$  is the filter constant, is used.

A P-type controller is designed in the following for a system with the parameters listed in Table III.

Any control design method or method for stability analysis of single-phase system can be used to design the P-type controller. The controller actually is designed using the Bode plot. Fig. 9 shows the Bode plot of the equivalent single-phase system with and without the P-type current controller. The controller gain was set to  $k_p = 0.25$  which yields to a cross-over frequency of

2.2 kHz. This justifies the use of average mode current control as the switching frequency of 72kHz is considerably higher. According to Fig. 9, a gain of  $k_p = 0.25$  results in a phase margin of  $60^\circ$ . Due to the limited sampling frequency of 72 kHz and the dead time  $T_t = 13.9\mu$ s, introduced by the calculation time of the controller, a pronounced drop of the phase with increasing frequency can be observed. This verifies that the control loop has to be analyzed as sampled data system for a proper control design and cannot be treated as continuous system which is frequently done in order to simplify the controller design. A design neglecting the sampling effects would result in a control loop with considerably reduced phase margin which could finally cause instability of the rectifier system. At least the robustness of the controller is reduced.

#### A. Behavior in Case of Distorted or Unbalanced Mains Voltage

As already discussed a PLL can be used to derive sinusoidal reference voltages which are multiplied by the conductance  $G_e^*$  in case of a distorted mains voltage. The measured distorted actual mains voltages should, however, be used to implement the input voltage feed-forward part in order to prevent input current distortions. A deviation in the feedforward voltage results in an error voltage across the inductors and the impact on the current distortions are alleviated by the current controller. The particular behavior is equivalent to an error in the duty cycle which can be analyzed using the disturbance transfer function  $F_d(s)$  which will be discussed below.

Due to the missing neutral wire connection the mains voltages (and therefore also their fundamental component) satisfy the condition

$$v_{N1} + v_{N2} + v_{N3} = 0 \quad (19)$$

also in the case where the three phase voltage magnitudes are not equal. The proposed method using the conductance  $G_e^*$  results in unbalanced input currents and a pulsating power flow from the grid to the dc-link occurs. A balancing method could be applied if balanced input currents are required.

#### B. Consideration of EMI-Filter and Mains Impedance

The discussed control loop relies on an ideally sinusoidal voltage source connected to the ac-side of the boost inductors. An EMI filter has, however, to be connected to the input of the rectifier circuit in order to comply with existing EMI standards and also the impedance of the grid which can in a first approach be modeled by an inductor  $L_M$  must be considered. The EMI filter tends to increase the amount of cross coupling and also some coupling between the filter stages exists [23]. A careful construction and arrangement of the EMI filter components, however, limits these additional couplings. Neglecting these cross couplings allows to draw a single-phase equivalent circuit of the EMI filter as shown in Fig. 10(a) for a three-stage EMI filter. Such a filter is used in the implemented hardware prototype of the  $\Delta$ -switch rectifier. The impedance of the EMI filter and of the mains shall be considered for the controller design and an equivalent circuit as shown in Fig. 10(b) can be

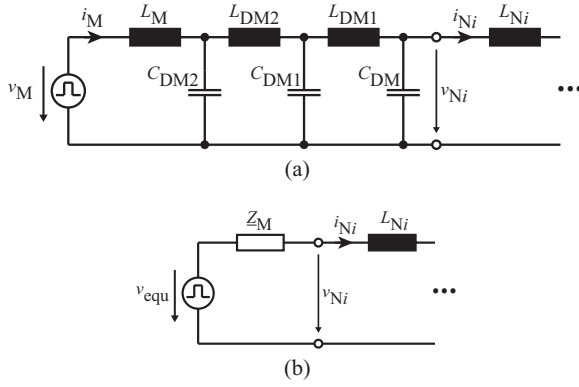


Fig. 10. (a) Equivalent single-phase circuit of the  $\Delta$ -switch rectifier input including differential mode EMI filter and mains impedance  $L_M$  and (b) simplified equivalent circuit which can be used for controller design.

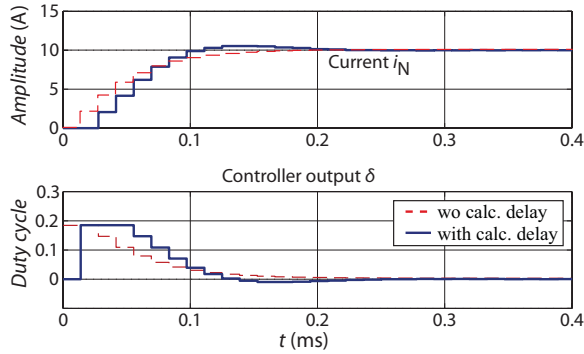


Fig. 11. Simulated response to a current reference step  $i_N = 0 \rightarrow 10$  A and controller output of the equivalent single-phase system.

calculated. The impedance  $Z_M$  has finally to be considered in (2) and may decrease the performance of the resulting control loop. This is not done here for the sake of a simple model.

## V. CONTROLLER PERFORMANCE

In the following, the  $\Delta$ -switch rectifier system is used together with the designed P-type controller to simulate the performance of the proposed control strategy. Fig. 11 shows the step response of the digitalized single-phase system for a step of  $i_{N1} = 10$  A, if cross couplings from/to the other phases are not considered. Two curves are shown in Fig. 11, one considering the calculation delay of the digital controller and one without consideration of this delay. An overshoot of only 5% can be observed for the curve considering the calculation delay. In addition, the controller output (duty cycle  $\delta$ ) is plotted.

The simplified controller design using the DNA method ensures only stability of the MIMO control but gives no information on the performance of the coupled system. The performance must therefore be checked by examining the system behavior using simulation tools. The impact of the calculation delay as shown in Fig. 11 is not considered in the following analysis of the coupled system. The system dynamic will therefore be similar to those of the single phase system without consideration of this delay.

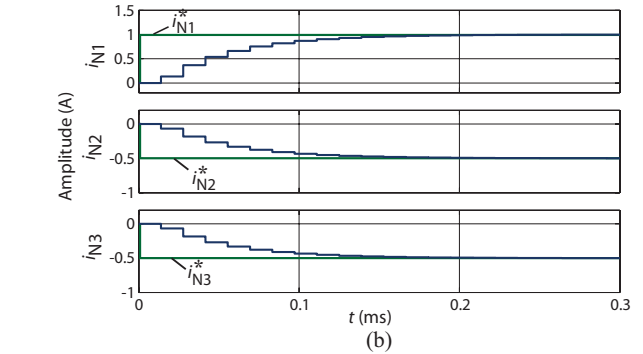
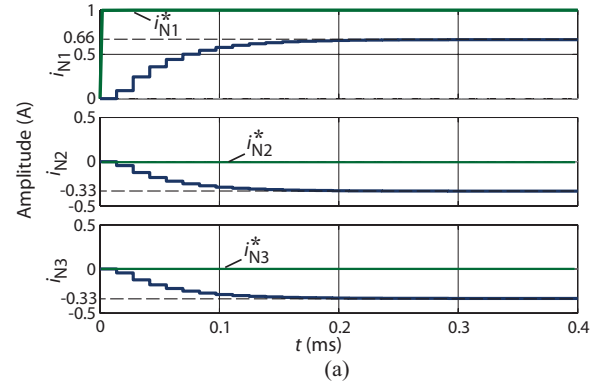


Fig. 12. Simulated response of the MIMO control system for a (a) forced current step of only  $i_{N1}^*$  to 1 A and (b) of  $i_{N1}^*$  to 1 A and  $i_{N2}^*, i_{N3}^*$  to  $-0.5$  A.

Using the designed current controller  $\mathbf{K}(s)$ , the MIMO control transfer function

$$\begin{aligned} \mathbf{T}(s) &= \frac{\mathbf{i}_N(s)}{\mathbf{i}_N^*(s)} = \mathbf{G}(s)\mathbf{K}(s)\mathbf{F}(s)^{-1} = \\ &= \frac{k_p k_{pwm} V_o}{sL_N + k_{pwm} k_p k_m V_o} \frac{1}{3} \begin{pmatrix} 2 & -1 & -1 \\ -1 & 2 & -1 \\ -1 & -1 & 2 \end{pmatrix} \quad (20) \end{aligned}$$

can be calculated where  $\mathbf{F}(s)$  is the return difference matrix defined in (15). Note that the calculation delay is not considered here. With this transfer function the step response of the MIMO rectifier system on a step only in  $i_{N1}$  is analyzed. The responses of the three input currents are depicted in Fig. 12(a). Such a current step is in practice not possible due to  $i_{N1} + i_{N2} + i_{N3} = 0$  and accordingly a response of all three phases can be observed. The response is, however, useful to study the influence of a control action in one phase on the other two phases. According to Fig. 12(a), the input current  $i_{N1}$  reaches only an amplitude of 0.66 and the two remaining phases show a response in negative direction. Both responses show the same time constants which can also be verified by inspecting the elements of  $\mathbf{T}(s)$ . A control action in one phase therefore intrinsically affects the two other phases. Note that the system response, e.g., settling time of the coupled system given in Fig. 12(a) is as expected slightly different to the system response of the single phase system shown in Fig. 11.

Fig. 12(b) shows the step response of the input currents for reference values not violating  $i_{N1} + i_{N2} + i_{N3} = 0$ . A step of

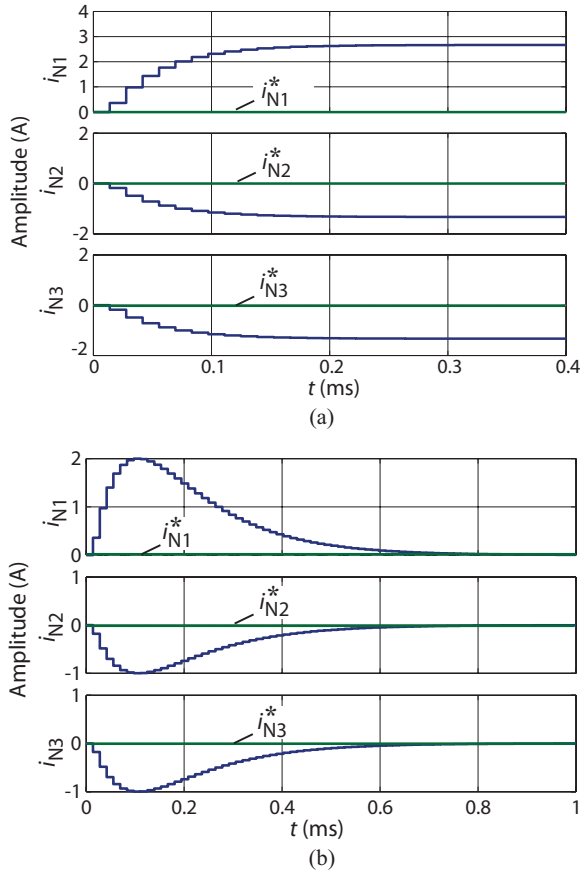


Fig. 13. Simulated step responses of the MIMO control system to a disturbance in the duty cycle  $w_{d1} = 0.33$  using (a) P-type controller ( $k_p = 0.25$ ) and (b) PI-type controller  $k_p = 0.25$ ,  $T_N = 0.2$  ms).

$i_{N1}^*$  to 1 A and  $i_{N2}^*$ ,  $i_{N3}^*$  to  $-0.5$  A is performed. Quite evidently, the system response shows the same time constants with the difference that no steady-state control errors occur. This verifies that the proposed control approach using three independent SISO controllers is well suited to control the coupled three-phase system.

According to Fig. 6 also the disturbance transfer function

$$\begin{aligned} \mathbf{F}_d(s) &= \frac{\mathbf{w}_d(s)}{\mathbf{i}_N(s)} = \mathbf{G}(s)\mathbf{F}(s)^{-1} = \\ &= \frac{k_{pwm}V_o}{sL_N + k_{pwm}k_p k_m V_o} \frac{1}{3} \begin{pmatrix} 2 & -1 & -1 \\ -1 & 2 & -1 \\ -1 & -1 & 2 \end{pmatrix} \quad (21) \end{aligned}$$

can be calculated. The simulated response of the rectifier system to a step in  $w_{d1} = 0.33$  is plotted in Fig. 13(a). As well known from single-phase systems a P-type controller cannot fully compensate such distortions. According to Fig. 13(a), this is also true for the  $\Delta$ -switch rectifier system.

A PI-type controller would be able to compensate this disturbances and the simulated system response to a step in  $w_{d1}$  using a PI-type controller ( $k_p = 0.25$ ,  $T_N = 0.2$  ms) is shown in Fig. 13(b). The PI-type controller, however, shows a tracking

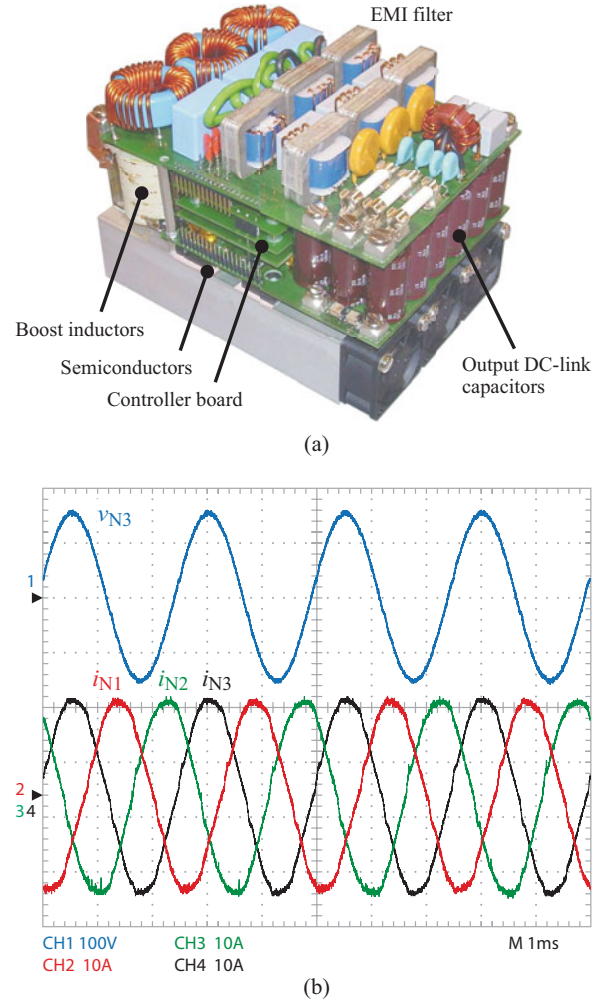


Fig. 14. (a) Constructed 5-kW  $\Delta$ -switch laboratory prototype and (b) measured input currents and phase voltage under continuous operation condition at  $V_{LL} = 200$  V,  $f_N = 400$  Hz and  $P_o = 4$  kW ( $\text{THD}_i = 2.3\%$ ,  $\lambda = 0.999$ ); CH1: mains voltage  $v_{N3}$ , 100 V/Div; CH2-CH4: phase currents, 10 A/Div; timebase: 1 ms.

error for line-frequency signals and generates distortions in the vicinity of the zero crossings as discussed in Section VI.

## VI. EXPERIMENTAL RESULTS

The constructed rectifier system shown in Fig. 14(a) is used to verify the designed control approach. The constructed hardware prototype is designed for a mains voltage of 200 V and an output power of 5 kW. In order to illustrate the good performance of the system the measured input currents at steady-state condition for a mains frequency of 400 Hz, as it may occur in an aircraft, and an output power of 4 kW are given in Fig. 14(b). The currents show sinusoidal shape and are in phase with the mains voltages where only phase voltage  $v_{N3}$  is shown in Fig. 14(b). The measured  $\text{THD}_i$  of 2.3% and the measured power factor of 0.999 verify the good performance of the controller during steady-state condition.

In order to verify the dynamic behavior of the three current controllers the particular step responses have been measured. The step is performed by increasing/decreasing the reference

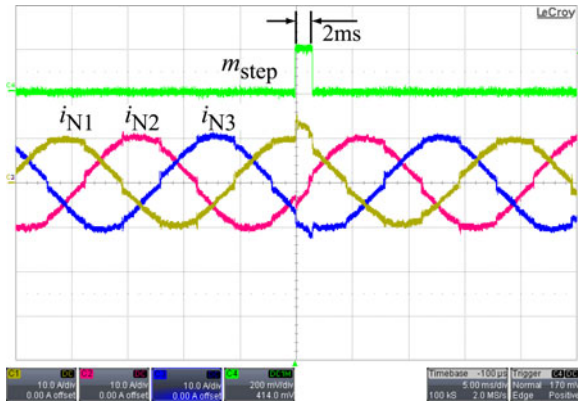
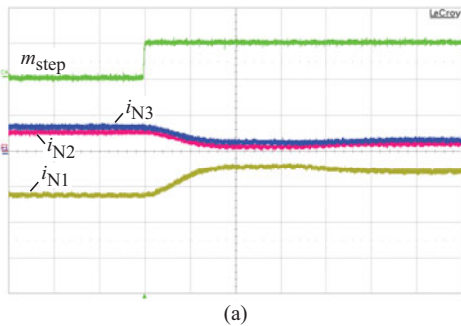
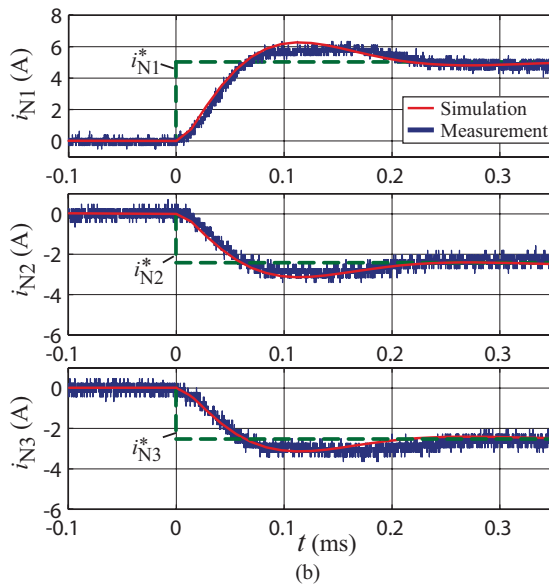


Fig. 15. Measured response of the rectifier system on a step of  $i_{N1} = 3.5$  A and  $i_{N2} = i_{N3} = -1.75$  A at  $\varphi_N = 160^\circ$ . The step is performed by increasing/decreasing the reference current for a duration of 2 ms (the corresponding control signal is marked with  $m_{step}$ ). Ch1:  $i_{N1}$ , 10 A/Div; Ch2:  $i_{N2}$ , 10 A/Div; Ch3:  $i_{N3}$ , 10 A/Div; Ch4:  $m_{step}$ , 200 mV/Div; time scale: 5 ms/Div.



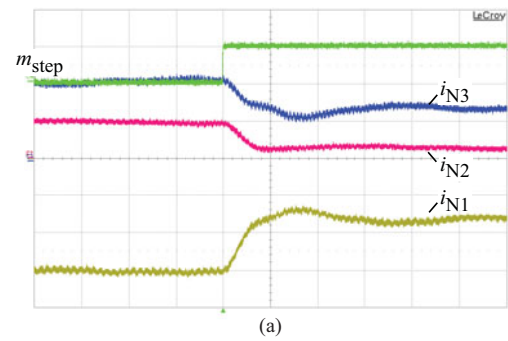
(a)



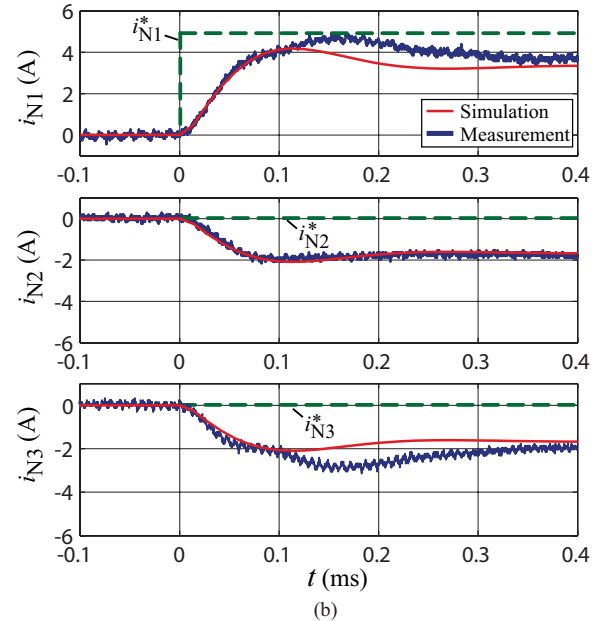
(b)

Fig. 16. Measured response of the control loop on a step of  $i_{N1}^* = 5$  A and  $i_{N2}^* = i_{N3}^* = -2.5$  A. (a) Measured signals: Ch1:  $i_{N1}$ , 5 A/Div; Ch2:  $i_{N2}$ , 5 A/Div; Ch3:  $i_{N3}$ , 5 A/Div; Ch4:  $m_{step}$ , 200 mV/Div; time scale: 50  $\mu$ s/Div. (b) Comparison of measured currents without fundamental component with results obtained by simulation.

current for a duration of 2 ms as shown in Fig. 15 (system operated at 50 Hz). The corresponding control signal is marked with  $m_{step}$ . The current step is added during operation with an



(a)



(b)

Fig. 17. Measured response of the control loop on a step only in  $i_{N1}^*$  (i.e.  $i_{N1}^* = 5$  A and  $i_{N2}^* = i_{N3}^* = 0$  A). (a) Measured signals: Ch1:  $i_{N1}$ , 2 A/Div; Ch2:  $i_{N2}$ , 2 A/Div; Ch3:  $i_{N3}$ , 2 A/Div; Ch4:  $m_{step}$ , 200 mV/Div; time scale: 100  $\mu$ s/Div. (b) Comparison of measured currents without fundamental component with results obtained by simulation.

output power of  $P_o = 2.4$  kW in order to prevent discontinuous mode of operation which may occur due to the unidirectional behavior of the rectifier system. Due to the short duration of the current step and due to the slow dynamic of the dc-bus voltage controller the output voltage increases only slightly and interactions between the dc-bus voltage controller and the current controller do not occur.

Fig. 16 shows the step response of the current control loop on a step of  $i_{N1}^* = 5$  A and  $i_{N2}^* = i_{N3}^* = -2.5$  A while the system is operating with an output power of  $P_o = 1.57$  kW. While Fig. 16(a) shows the original measurement, the 50-Hz component caused by the operating point of the rectifier system has been removed in Fig. 16(b) and the experimental results are compared to results provided by simulation using the derived model of the rectifier. In contrast to the results discussed in Section V (cf., Figs. 12 and 13) the calculation delay and also the measurement filter with  $T_M = 5 \mu$ s is considered in the simulated waveform which results in a tolerable overshoot. The measured currents are in good agreement with the simulation

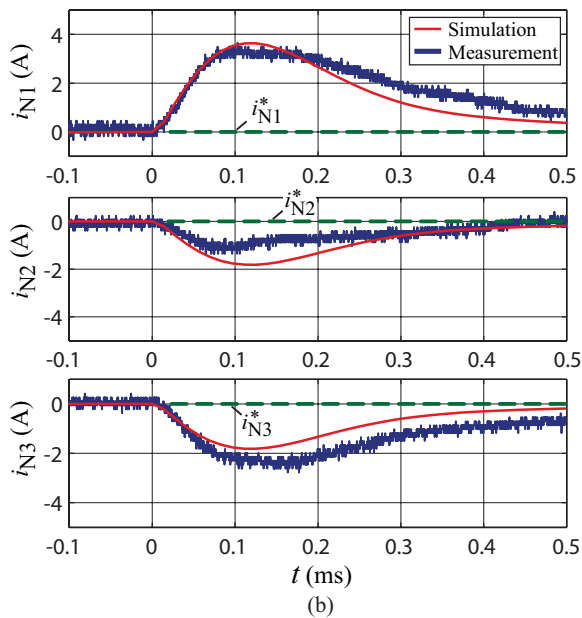
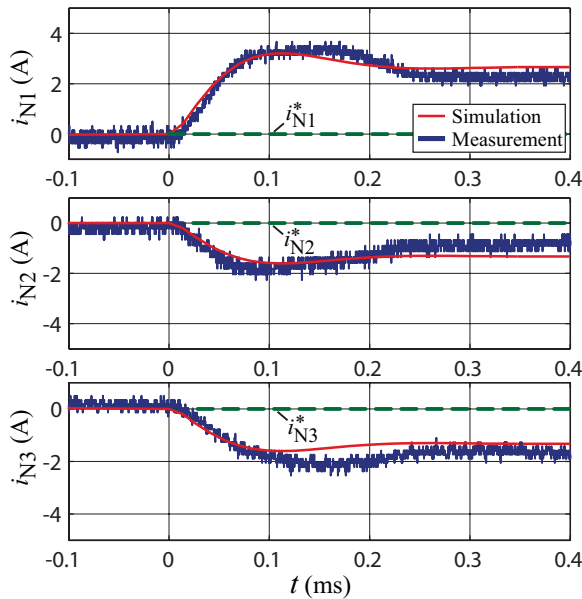


Fig. 18. Measured disturbance behavior of the control loop on a step in  $w_{d11} = 0.3$  and  $w_{d12} = w_{d13} = -0.15$  using (a) P-type controller with  $k_p = 0.25$  and (b) PI-type controller with the parameters  $k_p = 0.25$  and  $T_N = 0.2$  ms.

results which confirms the proposed simplified controller design neglecting the cross couplings of the converter system.

In Fig. 17, the response of the control system on a step only in  $i_{N1}^*$ , i.e.  $i_{N1}^* = 5$  A and  $i_{N2}^* = i_{N3}^* = 0$  A is shown. Such a step is not possible due to  $i_{N1} + i_{N2} + i_{N3} = 0$  and as shown in Fig. 17(b) a steady-state deviation occurs.

The disturbance behavior of the designed controller is tested by adding a step signal directly to the modulation signals as shown in Fig. 6. The measured results using a P-type controller are given in Fig. 18(a) where the 50-Hz component has already been removed. The P-type controller is not able to fully remove the control error and the expected steady state deviation remains. In Fig. 18(b), the measured disturbance behavior using a

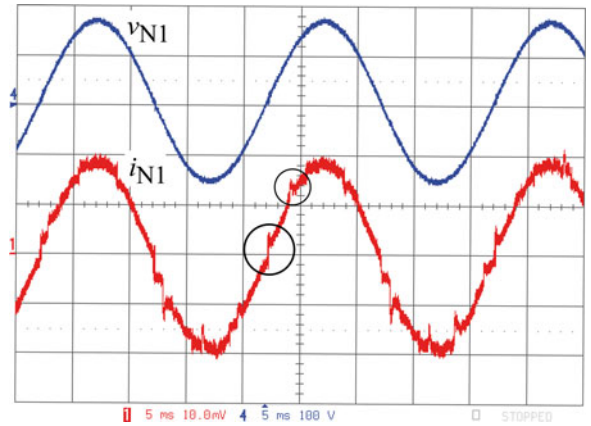


Fig. 19. Measured input current  $i_{N1}$  and input voltage  $v_{N1}$  taken from the implemented laboratory prototype if a PI-type current controller is used ( $V_{LL} = 200$  V,  $f_N = 50$  Hz,  $P_o = 2.5$  kW); CH1:  $i_{N1}$ , 10 A/Div; CH4:  $v_{N1}$ , 100 V/Div; timebase: 5 ms.

PI-type controller with the parameters  $k_p = 0.25$  and  $T_N = 0.2$  ms is shown. Due to the integral controller part the disturbance is fully compensated. A PI-type controller seems to be a better solution for implementing from this point of view. Next to the problem, that the PI-type controller does not show ideal tracking for 50/60-Hz signals, which could basically be achieved using a P+Resonant controller, the PI-type controller furthermore generates distortions in the vicinity of the zero crossings. Directly after a zero crossing the integral part of the controller shows a wrong sign and has to be reduced by an according control error (with the integrator time constant  $T_N$ ). The resulting (wrong) duty cycle yields to input current distortions. Fig. 19 shows a measurement result taken from the implemented laboratory prototype using a PI-type controller. Rather large distortions in the vicinity of the zero crossings can be observed. In addition, due to the cross couplings of the rectifier system, the zero-crossing distortions of the two other phases are evident (every  $60^\circ$ ). An implementation of a zero-crossing detection, which allows to reset the integral part of the PI-type controller directly after a zero crossing occurred, would be a possibility to reduce this negative effect [24]. The system operation, however, then depends on the correct detection of the zero crossings which should be omitted in order to achieve a robust current control behavior.

Overall, the implemented controller using three independent current controllers by neglecting the cross couplings shows good dynamic behavior and the experimental results are in good agreement with the results obtained by simulation using the derived converter model.

## VII. CONCLUSION

Using the three-phase  $\Delta$ -switch rectifier system, it has been shown that three independent current controllers, one designed for each phase, can under consideration of some boundary conditions be used to control the coupled three-phase rectifier system. This simplifies the controller design and eliminates the transfer of the system in a stationary frame or in a synchronous rotating  $dq$ -frame. The reason, why this simple approach can be

applied has been found in the loose cross couplings of the MIMO transfer function  $\mathbf{G}(s)$  of three-phase rectifier systems. As shown in this paper, the Gershgorin-theorem can be used to determine whether the use of three independent controllers is possible or not. The method has been derived using the three-phase  $\Delta$ -switch rectifier system, but is not limited to this topology and can be used for any three-phase rectifier of inverter system.

#### APPENDIX

In the following, the DNA method will be discussed briefly; the interested reader is referred to [18] for further details. The DNA method is an extension from the Nyquist stability and design criterion for SISO systems. The design approach uses the return difference matrix

$$\mathbf{F}(s) = [\mathbf{I} + \mathbf{G}(s)\mathbf{K}(s)\mathbf{M}(s)] \quad (22)$$

which would be a diagonal matrix in case of a fully decoupled system. As for single-phase control systems the poles of the multivariable control system are decisive for stability which can be calculated by solving the characteristic equation

$$\det[\lambda_{F_i}\mathbf{I} + \mathbf{G}(s)\mathbf{K}(s)\mathbf{M}(s)] = 0. \quad (23)$$

The eigenvalues  $\lambda_{F_i}$  are not equal to the diagonal elements  $F_{ii}$  in case of a coupled control loop and the cross-couplings directly take effect on the eigenvalues. The larger the cross couplings the larger the difference between the eigenvalues  $\lambda_{F_i}$  and the diagonal elements  $F_{ii}$ . The amount of cross couplings can be estimated using the Gershgorin theorem which states that the eigenvalues of the return difference matrix  $\mathbf{F}(s)$  are located in bands with the frequency dependent radii

$$D_i(j\omega) = \sum_{j=1, j \neq i}^m |F_{ij}(j\omega)|. \quad (24)$$

The return difference matrix  $\mathbf{F}(s)$  is called diagonally row dominant if

$$|F_{ii}(j\omega)| > \sum_{j=1, j \neq i}^m |F_{ij}(j\omega)| \quad (25)$$

and diagonally column dominant if

$$|F_{ii}(j\omega)| > \sum_{j=1, j \neq i}^m |F_{ji}(j\omega)| \quad (26)$$

applies.

According to [18] the following stability criterion can be derived:

*The control loop, using decoupled SISO controllers designed according to the main diagonal elements  $G_{ii}$ , is stable if  $\mathbf{F}(s)$  is either diagonally row dominant or diagonally column dominant and if the transfer functions  $G_{ii}(s)K_{ii}(s)M_{ii}(s)$  for  $i = 1, 2, \dots, m$  encircles the critical point  $-1 - n^+$ -times clockwise where  $n^+$  is the number of poles of  $G_{ii}(s)K_{ii}(s)M_{ii}(s)$  located in the right half-plane.*

This stability criterion is, however, only sufficient which means that the control loop may also be stable if the criterion is not fulfilled.

Based on this stability criterion Rosenbrock derived the so called DNA method [19]:

Assumptions:

- 1) The controlled system  $\mathbf{G}(s)$  is a system without direct feedthrough.
- 2)  $\mathbf{G}(s)$  is approximately diagonal row or column dominant.
- 3)  $\mathbf{G}(s)$  is bounded input bounded output (BIBO) stable.

DNA design method:

- 1) Design of  $m$  single-phase controllers  $K_{ii}(s)$  which show, together with the diagonal elements  $G_{ii}(s)$  and  $M_{ii}(s)$ , the desired transfer characteristic.
- 2) Check if the return difference matrix is diagonal row dominant [cf., (25)] or diagonal column dominant [cf., (26)].
- 3) If 1) and 2) are fulfilled the resulting multivariable control system is stable. Otherwise, the controller  $\mathbf{K}(s)$  has to be altered as long as 2) can be satisfied.
- 4) The control quality of the resulting multivariable control system has to be checked using simulation tools.

The stability margin of the designed control loop can be estimated using the distance of  $F_{ii}(j\omega)$  to the critical point  $-1$  were the Gershgorin bands around  $F_{ii}(j\omega)$  have to be considered. The stability margin can hence be analyzed using

$$\frac{D_i(j\omega)}{|1 + K_i(j\omega)G_{ii}(j\omega)|} = \frac{\sum_{j=1, j \neq i}^m |F_{ij}(j\omega)|}{|F_{ii}(j\omega)|}. \quad (27)$$

#### REFERENCES

- [1] RTCA Inc., *Environmental Conditions and Test Procedures for Airborne Equipment—RTCA DO-160F*. RTCA Inc. Std. (2007). [Online]. Available: <http://www.rtca.org>
- [2] J. W. Kolar and T. Friedli, "The essence of three-phase PFC rectifier systems," in *Proc. IEEE 33rd Int. Telecom. Energ. Conf.*, Oct. 2011, pp. 1–27.
- [3] J. W. Kolar and F. C. Zach, "A novel three-phase utility interface minimizing line current harmonics of high-power telecommunications rectifier modules," *IEEE Trans. Ind. Electron.*, vol. 44, no. 4, pp. 456–467, Aug. 1997.
- [4] M. Hartmann, J. Miniboeck, H. Ertl, and J. Kolar, "A three-phase delta switch rectifier for use in modern aircraft," *IEEE Trans. Ind. Electron.*, vol. 59, no. 9, pp. 3635–3647, Sep. 2012.
- [5] M. P. Kazmierkowski and L. Malesani, "Current control techniques for three-phase voltage-source PWM converters: A survey," *IEEE Trans. Ind. Electron.*, vol. 45, no. 5, pp. 691–703, Oct. 1998.
- [6] M. Malinowski, M. Jasinski, and M. P. Kazmierkowski, "simple direct power control of three-phase PWM rectifier using space-vector modulation (DPC-SVM)," *IEEE Trans. Ind. Electron.*, vol. 51, no. 2, pp. 447–454, Apr. 2004.
- [7] G. Escobar, A. M. Stankovic, J. M. Carrasco, E. Galvan, and R. Ortega, "Analysis and design of direct power control (DPC) for a three phase synchronous rectifier via output regulation subspaces," *IEEE Trans. Power Electron.*, vol. 18, no. 3, pp. 823–830, May 2003.
- [8] Y. Ye, M. Kazerani, and V. H. Quintana, "Modeling, control and implementation of three-phase PWM converters," *IEEE Trans. Power Electron.*, vol. 18, no. 3, pp. 857–864, May 2003.
- [9] H. Mao, D. Boroyevich, and F. C. Y. Lee, "Novel reduced-order small-signal model of a three-phase PWM rectifier and its application in control design and system analysis," *IEEE Trans. Power Electron.*, vol. 13, no. 3, pp. 511–521, May 1998.
- [10] R.-J. Tu and C.-L. Chen, "A new space-vector-modulated control for a uni-directional three-phase switch-mode rectifier," *IEEE Trans. Ind. Electron.*, vol. 45, no. 2, pp. 256–262, Apr. 1998.
- [11] L. Malesani, P. Mattavelli, and P. Tomasin, "Improved constant-frequency hysteresis current control of VSI inverters with simple feedforward bandwidth prediction," *IEEE Trans. Ind. Appl.*, vol. 33, no. 5, pp. 1194–1202, Sep./Oct. 1997.
- [12] C. Qiao and K. M. Smedley, "A general three-phase PFC controller for rectifiers with a parallel-connected dual boost topology," *IEEE Trans. Power Electron.*, vol. 17, no. 6, pp. 925–934, Nov. 2002.

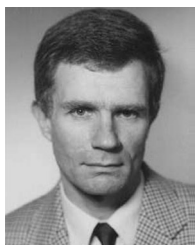
- [13] C. Qiao and K. M. Smedley, "A general three-phase PFC controller for rectifiers with a series-connected dual-boost topology," *IEEE Trans. Ind. Appl.*, vol. 38, no. 1, pp. 137–148, Jan./Feb. 2002.
- [14] J. C. Salmon, "Reliable 3-phase PWM boost rectifiers employing a stacked dual boost converter subtopology," *IEEE Trans. Ind. Appl.*, vol. 32, no. 3, pp. 542–551, May/Jun. 1996.
- [15] M. Chen and J. Sun, "Feedforward current control of boost single-phase PFC converters," *IEEE Trans. Power Electron.*, vol. 21, no. 2, pp. 338–345, Mar. 2006.
- [16] V. Kaura and V. Blasko, "Operation of a phase locked loop system under distorted utility conditions," *IEEE Trans. Ind. Appl.*, vol. 33, no. 1, pp. 58–63, Jan./Feb. 1997.
- [17] M. Hartmann, "Ultra-compact and ultra-efficient three-phase PWM rectifier systems for more electric aircraft," Ph.D. dissertation, Eidgenössische Technische Hochschule Zürich, Zurich, Switzerland, 2011.
- [18] J. Lunze, *Regelungstechnik 2, Mehrgroessensysteme, Digitale Regelung*. Berlin, Germany: Springer-Verlag, 1997.
- [19] H. Rosenbrock, *Computer-Aided Control System Design*. New York: Academic Press, 1981.
- [20] Y. Duan and H. Jin, "Digital controller design for switchmode power converters," in *Proc. 14th Ann. Appl. Power Electron. Conf. Exp.*, 1999, vol. 2, pp. 967–973.
- [21] M. Hartmann, S. Round, H. Ertl, and J. Kolar, "Digital current controller for a 1 MHz, 10 kW three-phase VIENNA rectifier," *IEEE Trans. Power Electron.*, vol. 24, no. 11, pp. 2496–2508, Nov. 2009.
- [22] D. M. V. D. Syde, K. D. Gussemé, A. R. V. D. Bossche, and J. A. Melkebeek, "Small-signal z-domain analysis of digitally controlled converters," in *Proc. 35th Annu. IEEE Power Electron. Spec. Conf.*, Jun. 2004, vol. 6, pp. 4299–4305.
- [23] S. Wang, F. C. Lee, D. Y. Chen, and W. G. Odendaal, "Effects of parasitic parameters on EMI filter performance," *IEEE Trans. Power Electron.*, vol. 19, no. 3, pp. 869–877, May 2004.
- [24] P. Ide, "Dreiphasiger netzfreundlicher dreipunkt-gleichrichter zur speisung von gleichspannungszwischenkreisen," Ph.D. dissertation, University of Paderborn, Paderborn, Germany, 2002.



**Michael Hartmann** (M'11) received the B.S. degree (Hons.) and the M.Sc. degree (with Hons.) in electrical engineering from the University of Technology Vienna, Vienna, Austria, in 2005 and 2006, respectively, and the Ph.D. degree from the Power Electronic Systems Laboratory, Swiss Federal Institute of Technology, Zurich, Switzerland, in summer 2011, where his research was focused on active three-phase rectifier systems with ultrahigh switching frequencies for application in more electric aircraft.

He is currently with Schneider Electric, Drive Technology and Systems, Vienna, where he is involved in the research on high-efficiency three-phase power converter systems for low-voltage power drives. His research interests further include three-phase power conversion, electromagnetic interference, and switched-mode power amplifiers using multicell topologies.

Dr. Hartmann received the 2012 IEEE Power Electronics Society Transaction Prize Paper Award in 2012.



**Hans Ertl** (M'93) received the Dipl.-Ing. (M.Sc.) degree and the Ph.D. degree in industrial electronics from the University of Technology Vienna, Vienna, Austria, in 1984 and 1991, respectively.

Since 1984, he has been with the Vienna University of Technology, Vienna, where he is currently an Associate Professor with the Power Electronics Section of the Institute of Electrical Drives and Machines. He has performed numerous industrial and scientific research projects in the areas of field-oriented control of ac drive systems, switch-mode power supplies for welding and industrial plasma processes, and active rectifier systems. He is the author or coauthor of numerous scientific papers and patents. His current research activities are focused on switch-mode power amplifiers and multicell topologies, in particular, for the generation of testing signals, for active ripple current compensators, and for several applications in the area of renewable energy systems.



**Johann W. Kolar** (F10) received the M.Sc. and Ph.D. degrees (*summa cum laude/promotio sub auspiciis praesidentis rei publicae*) from the University of Technology Vienna, Vienna, Austria.

Since 1984, he has been an Independent International Consultant in close collaboration with the University of Technology Vienna, in the fields of power electronics, industrial electronics, and high performance drives. He has proposed numerous novel PWM converter topologies, and modulation and control concepts, e.g., the VIENNA Rectifier and the three-phase ac–ac sparse matrix converter. He has published more 350 scientific papers in international journals and conference proceedings and has filed 75 patents. He was appointed Professor and Head of the Power Electronic Systems Laboratory, Swiss Federal Institute of Technology, Zurich, Switzerland, February 1, 2001. The focus of his current research is on ac–ac and ac–dc converter topologies with low effects on the mains, e.g., for power supply of data centers, more-electric-aircraft and distributed renewable energy systems. Further main areas of research are the realization of ultracompact and ultraefficient converter modules employing latest power semiconductor technology (e.g., SiC), novel concepts for cooling and EMI filtering, multidomain/scale modeling/simulation and multiobjective optimization, physical model-based lifetime prediction, pulsed power, and ultrahigh speed and bearingless motors.

Dr. Kolar received the Best Transactions Paper Award of the IEEE Industrial Electronics Society in 2005, the Best Paper Award of the International Conference on Performance Engineering in 2007, the 1st Prize Paper Award of the IEEE Industrial Applications Society Industrial Power Converter Committee in 2008, the IEEE IECON Best Paper Award of the IES Power Electronics Technical Committee in 2009, the 2009 IEEE Power Electronics Society Transaction Prize Paper Award, and the 2010 Best Paper Award of the IEEE/ASME TRANSACTIONS ON MECHATRONICS. He also received an Erskine Fellowship from the University of Canterbury, New Zealand, in 2003. He initiated and/or is the founder/co-founder of four spin-off companies targeting ultrahigh speed drives, multidomain/level simulation, ultracompact/efficient converter systems, and pulsed power/electronic energy processing. In 2006, the European Power Supplies Manufacturers Association (EPSMA) awarded the Power Electronics Systems Laboratory of ETH Zurich as the leading academic research institution in Power Electronics in Europe. He is a Fellow of the IEEE and a Member of the IEEJ and of International Steering Committees and Technical Program Committees of numerous international conferences in the field (e.g., the Director of the Power Quality Branch of the International Conference on Power Conversion and Intelligent Motion). He is the founding Chairman of the IEEE Power Electronics Society Austria and Switzerland Chapter and Chairman of the Education Chapter of the European Power Electronics Association. From 1997 through 2000, he has been serving as an Associate Editor of the IEEE TRANSACTIONS ON INDUSTRIAL ELECTRONICS and since 2001 as an Associate Editor of the IEEE TRANSACTIONS ON POWER ELECTRONICS. Since 2002, he also is an Associate Editor of the *Journal of Power Electronics of the Korean Institute of Power Electronics* and a member of the Editorial Advisory Board of the *IEEJ Transactions on Electrical and Electronic Engineering*.